# Characteristics of a Photonic Bandgap Single Defect Microcavity Electroluminescent Device

Wei Dong Zhou, *Student Member, IEEE*, Jayshri Sabarinathan, *Student Member, IEEE*, Pallab Bhattacharya, *Fellow, IEEE*, Boaz Kochman, Erik W. Berg, Pei-Chen Yu, and Stella W. Pang, *Fellow, IEEE*

***Abstract*—A microcavity surface-emitting coherent electroluminescent device operating at room temperature under pulsed current injection is described. The microcavity is formed by a single defect in the center of a 2-D photonic crystal consisting of a GaAs-based heterostructure. The gain region consists of two 70- Å compressively strained $In_{0.15}Ga_{0.85}As$ quantum wells, which exhibit a spontaneous emission peak at 940 nm. The maximum measured output power from a single device is 14.4 $\mu$W. The near-field image of the output resembles the calculated TE mode distribution in a single defect microcavity. The measured far-field pattern indicates the predicted directionality of a microcavity light source. The light-current characteristics of the device exhibit a gradual turn-on, or a soft threshold, typical of single- or few-mode microcavity devices. Analysis of the characteristics with the carrier and photon rate equations yields a spontaneous emission factor $\beta \approx 0.06$.**

***Index Terms*—Defect mode, microcavity, photonic bandgap, surface emitting.**

## I. Introduction

IT IS NOW well known that spontaneous emission is not an intrinsic atomic property. It can be modified by tailoring the electromagnetic environment that the atom can radiate into. This was first realized by Purcell [1], who noted that the spontaneous emission rate can be enhanced for an atom placed inside a cavity with one of its modes resonant with the transition under consideration, and by Kleppner [2], who discussed the opposite case of inhibited spontaneous emission.

In bulk material, or in a large cavity, the photon density of states is a monotonic function and spontaneous emission occurs into a large number of states, which occupy a spectral region much larger than the spontaneous emission linewidth. In a conventional laser made of such materials, most of the spontaneous emission is lost to free space as radiation modes and only a small fraction couples to the resonant mode of the cavity formed by the mirrors. Therefore, significant stimulated emission output can only be obtained when the input power crosses a threshold to overcome the free-space loss. In a wavelength-sized microcavity [3]–[5], formed by 1-, 2-, or 3-D photon-mode confinement, the photon-mode density develops singularities, just as in the case of carrier confinement. In this case, a single spectrally distinct mode, determined by the microcavity dimensions, can receive most or all of the spontaneous emission.

Manuscript received January 9, 2001; revised May 17, 2001. This work was supported by the Office of Naval Research under Grant N000 014-96-1-0024 and by the Army Research Office (MURI program) under Grant DAAG55-98-1-0288.

The authors are with the Department of Electrical Engineering and Computer Science, University of Michigan, Ann Arbor, MI 48109-2122 USA.

Publisher Item Identifier S 0018-9197(01)07361-4.

By applying Fermi's golden rule, it has been shown that the rate of spontaneous emission is enhanced in such a microcavity, due to the change in the mode density [4]. The spatial profile of the spontaneous emission in the cavity plane has also been calculated, and it has been shown that the profile can become vertically collimated. This is easily seen in a planar microcavity, with confinement in one direction, but has also been theoretically shown in a wavelength sized microcavity created by lateral confinement and *without* high-reflectivity mirrors in the direction of the guided modes [6], [7].

The most appealing technique to realize a true photonic microcavity is to use a dielectric photonic crystal, realized with a periodic modulation of the dielectric constant [8], [9]. As lightwave scatters within a material with a periodic variation in the dielectric constant, destructive interference of certain frequencies, depending on geometry and index variation, produces a photonic bandgap (PBG) [10]. Photons whose energies lie within the gap cannot propagate through the structure. However, a point defect—a missing period or phase slip—in the structure will locally trap photons and create a microcavity [11]–[19]. All the photons corresponding to the wavelength of the defect, generated by recombination in the PBG crystal or otherwise, will be funneled into the single resonant mode of the defect and this mode can propagate in the crystal. Such a single-mode microcavity light-emitting diode, with a spontaneous emission factor $\beta \cong 1$, can also be viewed as a thresholdless laser. However, there are important differences. In a microcavity, or defect, there is feedback of the dominant mode in all directions. Also, unlike a laser, in which the output is a result of mode competition and gain saturation, in a true microcavity there is only one mode that is emitted. The resonant defect mode is highly localized around the defect and can either propogate in the plane of the PBG crystal by tunneling, or leak out in the vertical direction. Lasing with optical pumping from a microcavity formed by a single defect in the center of a disc-shaped photonic crystal has been demonstrated [18], [19] and we have recently reported room-temperature operation of a PBG microcavity surface emitting electroluminescent device [20]. Photon confinement and the modal properties of a PBG-based microcavity are quite similar to those of a reflector-based microcavity. However, the former relies on multiple reflections from distributed scatterers, instead of the multiple reflections from localized mirrors in the latter, which selects only those modes having in-phase multiple reflections and rejects all other electromagnetic modes.

In this paper, we report the characteristics of a GaAs-based single defect PBG electroluminescent device in detail. The

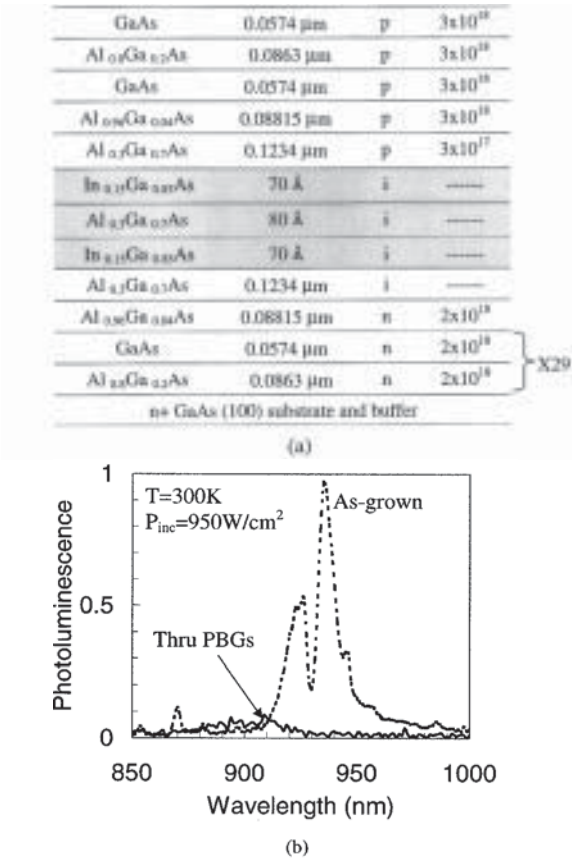


Fig. 1. (a) Device heterostructure grown by MOVPE on $n^+$ GaAs substrate with two 70 Å $In_{0.15}Ga_{0.85}As$–GaAs quantum wells in a $\lambda$-cavity. (b) Room-temperature PL spectra for an as-grown sample (dotted line) and for the 2-D PBG crystal without defect (solid line). Note that the suppression ratio is at least 20 dB for the PL intensity in the latter case.

single defect in a 2-D photonic crystal, formed of semiconductor heterostructures containing $In_{0.15}Ga_{0.85}As$–GaAs quantum wells, forms the microcavity. In particular, the light-current ($L$-$I$) characteristics are very different from conventional lasers, or even microcavity VCSELs. Data from the device also indicate that light emission truly occurs from the microcavity formed by the defect and not from the rest of the 2-D PBG. The device is, at best, a "few mode" LED. The concept of a threshold current, therefore, cannot be strictly applied, and instead, we see a gradual turn-on, exactly as described by Yokoyama [3]. However, for simplicity, we will refer to the current at the turn-on point as a threshold, even though the device may not operate as a laser. In fact, we have analyzed this by the appropriate carrier and photon rate equations and by taking into account the substantial nonradiative recombination at the air holes. Excellent agreement is obtained with experimental data. In what follows, the device design is described in Section II and device fabrication in Section III. The experimental results, together with analysis of the data are described in Section IV, followed by a discussion in Section V. The important results are summarized in Section VI.

## II. Design of PBG Crystal and Microcavity

Epitaxial growth and fabrication of the devices have been described by us elsewhere [20], but is briefly reiterated for completeness. The device heterostructure, grown by metal-organic vapor phase epitaxy (MOVPE), is shown in Fig. 1(a). It consists of an undoped cavity region of thickness $\lambda/n$ with two 70-Å pseudomorphic $In_{0.15}Ga_{0.85}As$ quantum wells in the middle and $p$-type $Al_{0.3}Ga_{0.7}As$ and contact layers on the top. $N$- and $p$-type $Al_{0.96}Ga_{0.04}As$ layers are inserted for lateral wet-oxidation during the processing of the device. Therefore, the heterostructure is similar to that of an oxide confined VCSEL [21], without the top distributed Bragg reflector (DBR) mirror. The reflectivity of the top surface is that provided by the semiconductor-air interface. Even the bottom DBR is not necessary, but was incorporated to achieve a high index step (reflectivity) in the bottom side and to ensure leakage of light from the top surface.

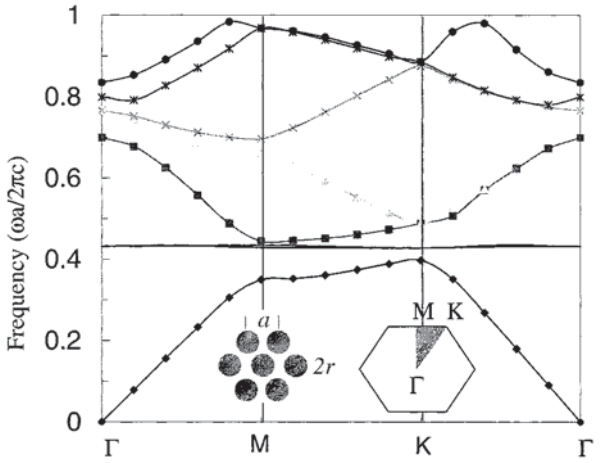


Fig. 2. Calculated TE bandstructure and defect-mode levels using plane wave expansion techniques for a 2-D hexagonal PBG crystal geometry with air-holes surrounded by a region with effective index of 1.8 (to account for the index steps in the $z$-direction of our finite 2-D slab) and $(r/a) = 0.32$. A single-defect mode centered in the bandgap at a normalized frequency $(a/\lambda) = 0.43$ corresponding to $a = 0.4\ \mu$m and $\lambda = 940$ nm is shown.

The cavity was designed with a 2-D PBG encompassing the peak emission wavelength at a normalized frequency of $a/\lambda$ for the TE modes. The calculated bandgap for the TE modes and the defect mode are shown in Fig. 2. The calculations were done in the frequency domain considering a 2-D geometry with an effective index to take into account the index steps in the vertical direction. The calculations are based on the plane-wave expansion method and effective medium theory [22]–[24]. While a unit cell was used in the perfect PBG, where circular air holes are arranged in a triangular lattice in a dielectric background with a dielectric constant of 12.5 (inset of Fig. 2), a supercell [24] must be used when a defect is introduced into an otherwise perfect PBG, where the structure is approximated with the discrete-translationally symmetric structure. Recalling that the electric field is primarily parallel to the interface for TE modes and perpendicular for TM modes, it is straightforward to understand that a dielectric tensor, which is valid for any polarization, can be generated in terms of the effective medium theory. In our case, the PBG center frequency $a/\lambda = 0.426$, which corresponds to the quantum-well peak emission wavelength of 0.94 $\mu$m. Values of $a$ and $r$, 0.4 and 0.13 $\mu$m, respectively, give the best experimental results, and we believe these dimensions place the quantum well emission within the PBG of the 2-D crystal. Some amount of trial and error was involved since only a quasi-3-D model was used.

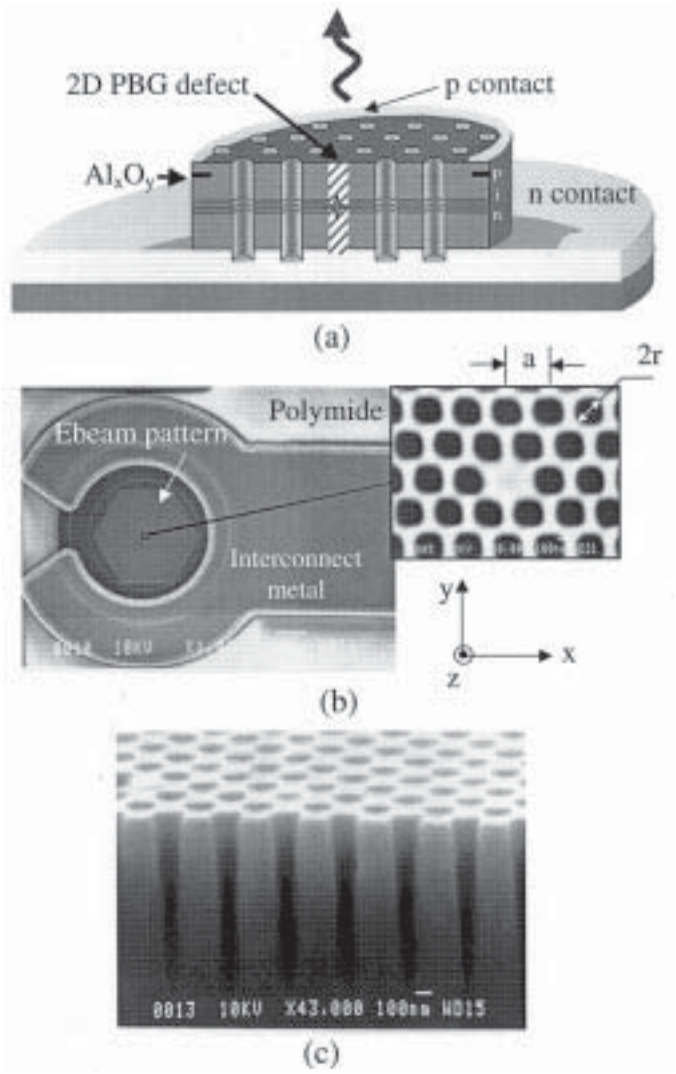


Fig. 3. (a) Schematic of the electrically injected photonic crystal surface-emitting light emitter with single defect forming the microcavity. (b) SEM images of top view of a fabricated device with top electrical ohmic contact surrounding the PBG with the single defect magnified in the inset. (c) Cross-sectional SEM image of the 2-D PBG slab, with deep etching through the cavity down to the bottom DBR region.

## III. Device Fabrication

Mesa-etched devices with p and n contacts were first fabricated by optical lithography, dry and wet etching, metallization, and polymide planarization. Lateral wet-oxidation [25] of the $Al_{0.96}Ga_{0.04}As$ layers was used here to funnel the charge carriers more efficiently into the center of the PBG region, which is next formed by e-beam lithography, pattern transfer, and deep dry etching techniques [26]. The window inside the oxide ring is measured to be $\sim$40 $\mu$m in diameter. A single defect in the center defines the $\lambda$-sized microcavity. The 0.8-$\mu$m deep etch goes through the entire cavity region and well into the bottom DBR to ensure a good overlap with the optical field. Dimensions of $r = 0.13$ and $a = 0.4$ $\mu$m define the final PBG microcavity.

A schematic of the complete device with $p$- and $n$-type contact metallizations are shown in Fig. 3, together with scanning electron microscope (SEM) images of the PBG and the defect. The active area aperture, created by the single defect, is surrounded by over 40 periods of PBG, having an extent (radius) of 20 $\mu$m, which also coincides with the current funneling aperture formed by wet oxidation of the $Al_{0.96}Ga_{0.04}As$ layers. Excellent diode characteristics were measured for the device at various stages. The reverse leakage current increased from 40 pA to 1 nA after formation of the PBG crystal.

Room-temperature photoluminescence (PL) measurements were also done on the as-grown heterostructures and on the samples after etching of air holes to form the PBG. The measurements were made with a 632-nm laser, 1-m scanning spectrometer, and a liquid-nitrogen cooled photomultiplier with lock-in amplification of the signal. The luminescence measured from the InGaAs quantum wells is shown in Fig. 1(b). This output is predominantly transverse-electric (TE) polarized due to the compressive strain in the InGaAs quantum wells. This is an advantage, since the PBG defect mode is predominantly TE polarized. It may also be noted that the peak intensity (940 nm) of the PL signal from the PBG region is at least ten times lower than that from the as-grown heterostructure. We also fabricated oxide-confined microcavity VCSEL-like devices with the epitaxial heterostructures before etching the air holes. No top DBR mirror was formed. These devices did not show lasing behavior. These control experiments are crucial in eliminating other possible sources of light emission that is subsequently observed in the devices with the PBG crystal with single defect.

## IV. Device Characteristics

The $L$-$I$ and spectral characteristics of the PBG microcavity devices were measured in the pulsed mode (1-$\mu$s width with 1% duty cycle) with probe contacts. The output was measured in a direction normal to the surface. It may be remembered that the dominant mode in the defect region can propagate laterally, or leak out vertically. The DBR mirror at the bottom helps in surface emission from the top. A turn-on, or soft threshold-like behavior in the injection current is consistently observed in the *L-I* characteristics (Fig. 4). We have observed a similar threshold-like behavior in 1.55-$\mu$m oxide-confined microcavity electroluminescent devices [27]. The maximum output power is 14.4 $\mu$W [Fig. 4(b)]. Care was taken to ensure that the measured power lies within the operating spectral and sensitivity regimes of the Ge detector, especially at low output powers. The measured spectral outputs at different injection currents, below and above the turn-on, or threshold, are shown in Fig. 5. The spectra at low injection currents, below the turn-on, are also characterized by several distinct peaks, rather than a broad output. From a lineshape analysis of the main peak at 931 nm (above threshold), we derive a linewidth of 8 Å, which leads to a quality factor $Q(\lambda/\delta\lambda)$ of $\sim$1164. This is, of course, different from the cold cavity $Q$, which we believe is lower in value. Our spectral data are also very noisy due to low output power, in addition to multimode behavior, thereby making the measurement of the linewidth less accurate. We estimate the $Q$ value to be $\sim$200, and the values of 300–500 for similar devices have been reported [18]. It may be noted that the vertical cavity $Q$ is very low ($\sim$12 in our case) since there is no DBR on the top surface. The peak output wavelength corresponds to a normalized frequency of 0.43, which is within

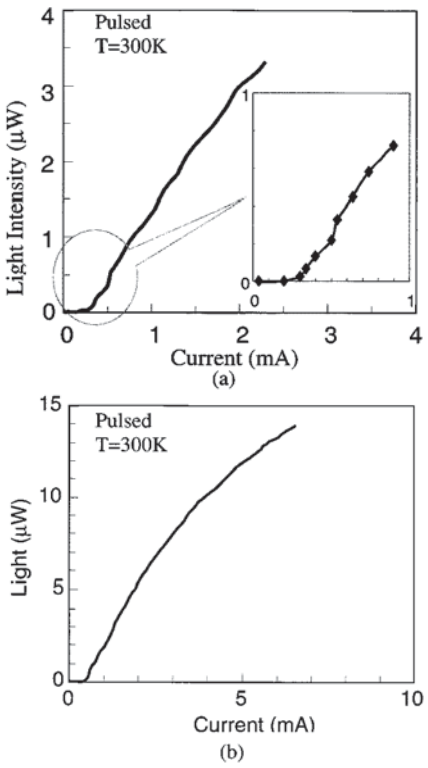


Fig. 4. $L$-$I$ characteristics of the single-defect PBG device at 300 K in pulsed mode showing: (a) "soft" threshold current of 300 $\mu$A and (b) maximum power output of 14.4 $\mu$W.

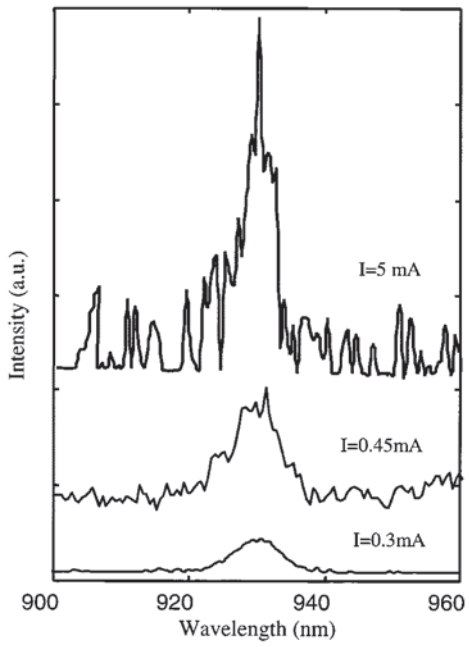


Fig. 5. Measured spectral outputs for the device at different biasing currents. The peak emission for the injection current of 5 mA is at 931 nm with a linewidth of $\sim$8 Å.

the bandgap of the photonic crystal incorporated in our device. While the PL emission peaks at 940 nm at 300 K, the output emission center wavelength is 931 nm. We believe the shift is mainly due to the process induced PBG position and defect level shift [28].

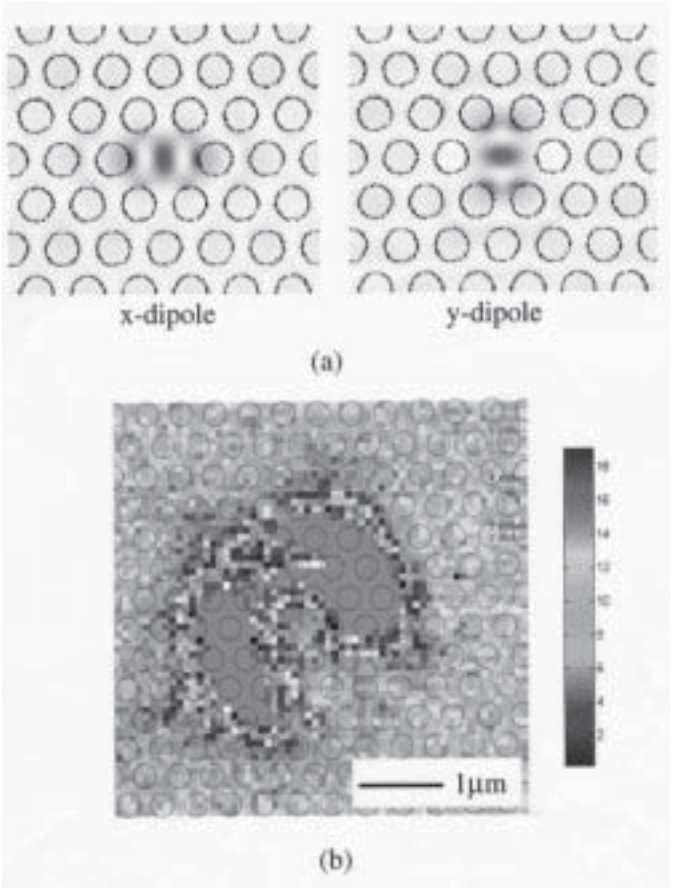


Fig. 6. (a) Calculated electric field energy distribution (TE) in a horizontal ($x$-$y$ plane) slice of the middle of the single-defect PBG crystal showing two degenerate modes localized in the single defect. (b) Measured near-field image of the device output superimposed on the 2-D air-hole photonic crystal pattern.

The field distribution and the localized defect mode in and around the defect in the photonic crystal were also calculated by the technique described in Section II. The computations reveal that most of the energy of the defect mode leaks in the vertical $(z)$ direction, rather than being guided in the plane ($x$-$y$) of the photonic crystal. The modes are predominantly TE, with a small contribution from unguided transverse magnetic (TM) modes. Fig. 6(a) shows the calculated dominant TE modes in the middle of the cavity for $x$ and $y$ dipole, respectively, which have a symmetrical distribution and extend radially through the first few periods of the air holes in the photonic crystal. The distribution is that of a pair of degenerate dipole modes, which may be present in the measured output spectrum of Fig. 5. We have also measured the near-field image [Fig. 6(b)] of the light output with a Spiricon Laser Beam Diagnostics system for an injection current of 2.2 mA, which is above threshold. The imaging was done at a distance of 4 mm from the surface of the device through an objective lens. It is evident that the modes spread out from the defect (microcavity) region during its propagation along the vertical direction. The nonuniformity in the mode profile is possibly due to light scattering in the air holes and diffraction at the surface [29]. Nonetheless, it is important to note that the 4-$\mu$m

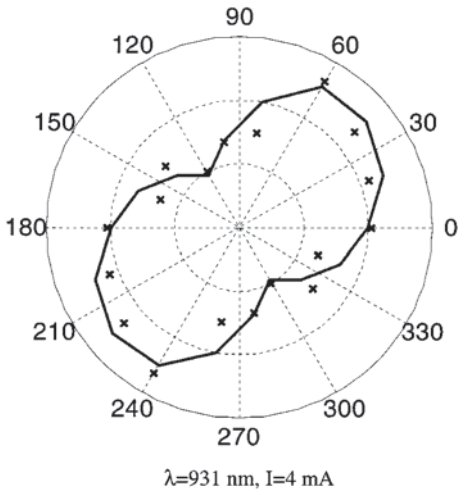


Fig. 7. Measured polarization characteristics of the device (at $\lambda = 931$ nm) for an injection current of 4 mA. It is evident that the output does not display a single definite polarization.

lateral extent of the near field image is much smaller than the oxide window diameter of 40 $\mu$m and further helps to exclude the possibility that the entire 2-D-PBG crystal beyond the defect microcavity contributes to the observed output. Ideally, there should be a rapid decay of the electromagnetic fields inside the PBG lattice. In our case, the fact that the measured near-field image extends out to five lattice periods implies a spreading out of some sort, and the image may not exactly map the real field distribution pattern inside the cavity.

It may also be noted that the quantum-well emission shown in Fig. 1(b) overlaps with the bottom of the air band at the $M$ point, and this emission can, therefore, couple with the air-band-guided modes propagating in the $\Gamma M$ direction. The near-field image indicates increased leakage in the $\Gamma M$ direction. However, it cannot be confirmed whether only the dipole defect mode or a combination of defect and air-band modes are observed.

Finally, we have also measured the far-field radiation pattern in devices with and without PBG crystal formation. The linewidth (full-width at half-maximum) of the pattern is $\sim$30°, in contrast to 90° for larger oxide-confined light-emitting diodes, confirming that the observed light output originates from the single-defect microcavity.

The enhancement in spontaneous emission due to the microcavity effect (Purcell factor) was estimated [30], [31] from the measured cavity $Q$ and a calculated effective modal volume $V_{\rm eff} \cong 3(\lambda/2n)^3$. An enhancement by a factor of 15 is derived based on the calculated effective modal volume.

The measured polarization characteristics of the device at an injection current of 4 mA is shown in Fig. 7. Although a preferential polarization direction can be easily identified, output is clearly not in one definite polarization state, which is in agreement with data reported from a similar defect mode laser with optical pumping [18]. We attribute the polarization behavior to the fact that the emission peak output consists of at least a pair of degenerate modes. By lowering the cavity symmetry [19], a single defect mode cavity can be formed and we expect a better-defined linearly polarized output.

## V. Discussions

Finally, it is important to try and understand the nature of the light output and whether a true threshold can be expected. The injected carriers reach the defect (microcavity) by traveling around the air-hole columns in the photonic crystal. Some carriers may also travel via the top surface. This region, defined by the wet-oxidized AlGaAs layers, is 40 $\mu$m in diameter. It can, therefore, be assumed that some fraction of the initial injection current is lost to nonradiative recombination, of which surface recombination is the dominant component. The surface recombination current can be expressed in terms of surface recombination velocity $S_0$ as [32]

$$I_S = qS_0(np)^{1/2}L_sL_p \tag{1}$$

where

$(np)^{1/2}$ carrier density at the surface;
$L_s$ surface diffusion length;
$L_p$ perimeter length of the interface.

By taking $S_0 = 10^6$ cm/s, $L_s = 1$ $\mu$m (total etch depth), $L_p = 2\pi r$ with $r = 0.13$ $\mu$m, we get values of the surface recombination current through the holes and on the surface to be 96 and 14 $\mu$A, respectively, adding to a total of 110 $\mu$A. Since the observed soft threshold occurs at a larger value of injection current, it is believed that, for injection currents larger than 110 $\mu$A, radiative recombination dominates.

It is also important and necessary to understand the nature of the $L$–$I$ characteristics, especially at and near the "soft" threshold, or turn-on, region. For a true microcavity, the number of modes is limited to one, or a few, and the value of the spontaneous emission factor $\beta$ is greatly enhanced. Theoretically, a microcavity light source formed by a single defect in a photonic crystal should have a near unity value of spontaneous emission factor $\beta$. We have analyzed the measured $L$-$I$ characteristics with the rate equations for carriers and photons in microcavity lasers [33]. The carrier density $N$ in the active region and the photon population $P$ in the cavity can be described by the following rate equations:

$$\frac{dN}{dt} = \frac{I}{qV} - \frac{N}{\tau_{\rm sp}} - \frac{N}{\tau_{\rm nr}} - \Gamma\frac{gP}{V} \tag{2a}$$

$$\frac{dP}{dt} = \Gamma\frac{gP}{V} - \frac{P}{\tau_p} + \beta\frac{NV}{\tau_{\rm sp}} \tag{2b}$$

where

$I$ injection current;
$q$ electron charge;
$V$ active region volume;
$\tau_{\rm nr}$ nonradiative recombination lifetime;
$\tau_{\rm sp}$ spontaneous emission lifetime;
$\tau_{\rm p}$ stimulated emission lifetime;
$\Gamma$ confinement factor;
$g$ carrier density dependent gain.

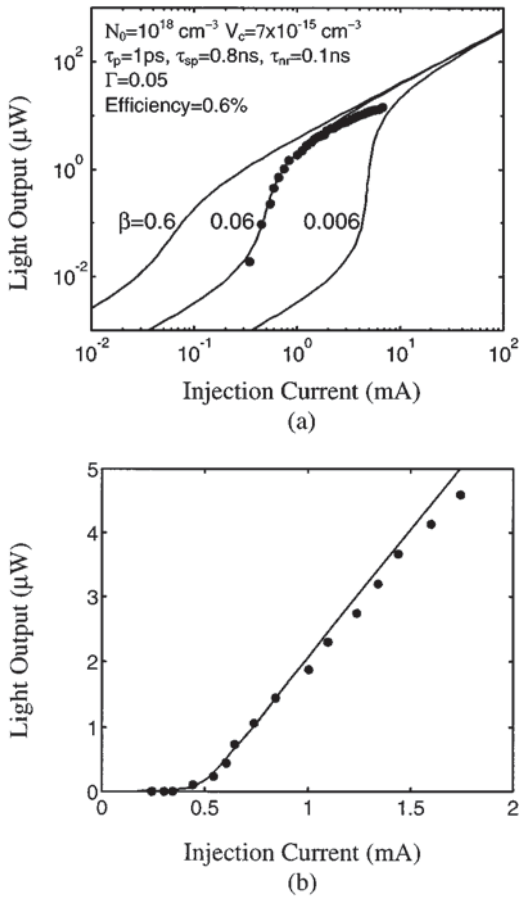


Fig. 8. Numerical fit of the measured $L$-$I$ characteristics (solid dots) to the calculated $L$-$I$ characteristics for a microcavity light emitter (solid lines), showing good agreement for a spontaneous emission factor $\beta = 0.06$, which indicates strong spontaneous emission control: (a) logarithmic and (b) linear scales.

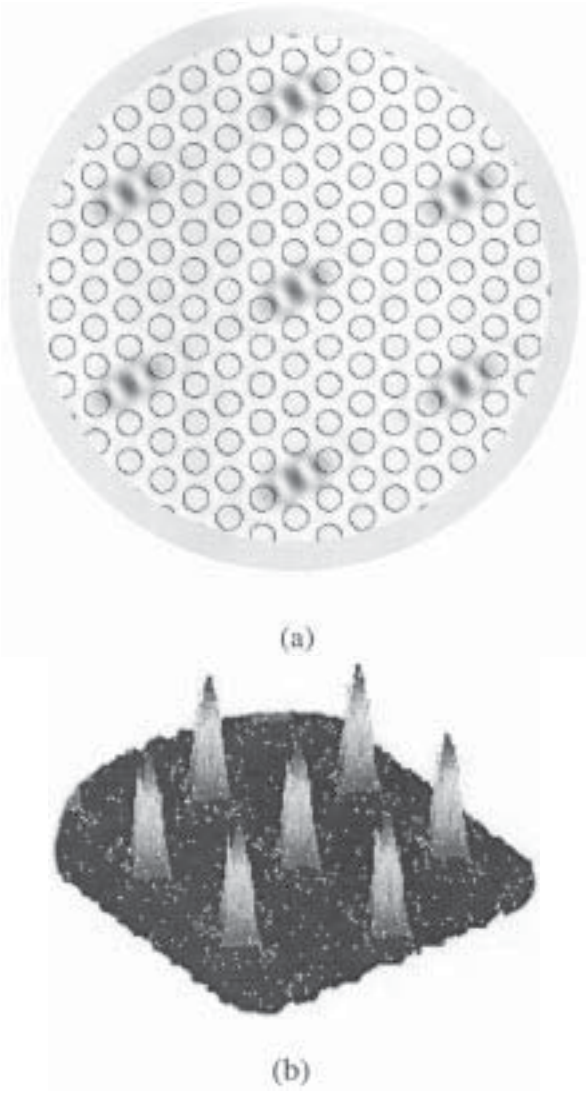


Fig. 9. (a) Schematic of a possible single defect PBG defect mode emitter array. (b) Calculated field distribution in the array. Note that the defect spacing for such an array can be as small as 4 $\mu$m, since theoretical calculations show that seven periods of air holes surrounding the single defect is enough to achieve more than 2-dB suppression of unwanted modes.

$g$ can be expressed in terms of the transparent carrier density $N_0$ and the differential gain as

$$g = \frac{dg}{dN}(N - N_0) = \frac{\beta V}{\tau_{\rm sp}}(N - N_0). \tag{3}$$

The steady-state solution of the rate equations yield the output $L$-$I$ characteristics. As can be seen in Fig. 8, good agreement between measured and calculated data is obtained for $\beta \cong 0.06$ by taking into account a relatively large nonradiative surface recombination induced carrier loss ($\tau_{\rm sp} \ll \tau_{\rm nr}$) and photon scattering loss in the device. A photon lifetime of 1 ps and an optical confinement factor of 0.05 are used in the analysis. It may be noted that the value of $\beta$, although less than unity, is significantly larger than that in conventional semiconductor lasers ($\beta \sim 10^{-4} - 10^{-5}$).

## VI. Conclusion

We report the characteristics of an electrically injected microcavity light emitter in which the mode-confining volume is defined by a single defect in a semiconductor-based PBG crystal. The bandgap of the photonic crystal is designed to contain the radiative emission from $In_{0.15}Ga_{0.85}As$–GaAs quantum wells, which form the gain medium.

Realization of the device reported here involves careful processing and low damage etching with a high aspect ratio. If the thickness of the PBG region is reduced, the TE field is less confined in the microcavity. The $L$-$I$ characteristics of the device exhibit a "soft" threshold, or turn-on, behavior, as expected from true microcavity light emitters. The light output results from all or most of the spontaneous emission being funneled into a few microcavity modes. From analysis of the data with appropriate carrier and photon rate equations, a value of $\beta = 0.06$ is derived. It is important to realize that the device need not have DBR mirrors; even the bottom mirror in our heterostructure is not required. The lithography and etch dimensions will be much larger and the tolerances much better for 1.55-$\mu$m emitters, using InP-based materials, which inherently have smaller surface recombination. Surface-emitting light emitters at this wavelength are technologically important for optical communications. In spite of a relatively large value of $\beta$, the output power is low. This is due to the small microcavity volume. However, a closely spaced array, as schematically shown in Fig. 9, will have

much higher—and at the same time collimated—power outputs. Such an array can also be designed to be multi-wavelength by simply varying the PBG crystal dimension [34], [35], which would be useful for dense WDM (DWDM) lightwave communication systems.

## REFERENCES


[1] E. M. Purcell, "Spontaneous emission probabilities at radio frequencies," *Phys. Rev.*, vol. 69, p. 681, 1946.

[2] D. Kleppner, "Inhibited spontaneous emission," *Phys. Rev. Lett.*, vol. 47, pp. 233–236, 1981.

[3] H. Yokoyama, "Physics and device applications of optical microcavities," *Science*, vol. 256, pp. 66–70, 1992.

[4] H. Benisty, J. Gerard, R. Hondre, J. Rarity, and C. Weisbuch, Eds., *Confined Photon Systems: Fundamentals and Applications*: Springer, 1999.

[5] T. Baba, "Photonic crystals and microdisk cavities based on GaInAsP-InP system," *IEEE J. Select. Topics Quantum Electron.*, vol. 3, pp. 808–830, 1997.

[6] I. Vurgaftman and J. Singh, "Spatial and spectral characteristics of spontaneous emission from semiconductor quantum wells in microscopic cylindrical cavities," *Appl. Phys. Lett.*, vol. 67, pp. 3865–3867, 1995.

[7] E. F. Schubert and N. E. J. Hunt, "Enhancement of spontaneous emission in microcavities," in *Vertical-Cavity Surface-Emitting Lasers: Design, Fabrication, Characterization, and Applications*, C. Wilmsen, H. Temkin, and L. A. Coldren, Eds. Cambridge, U.K.: Cambridge Univ. Press, 1999, pp. 68–107.

[8] E. Yablonovitch, "Inhabited spontaneous emission in solid-state physics and electronics," *Phys. Rev. Lett.*, vol. 58, pp. 2059–2062, 1987.

[9] ——, "Photonic band-gap structures," *J. Opt. Soc. Amer. B*, vol. 10, pp. 283–295, 1993.

[10] J. D. Joannopoulos, R. D. Meade, and J. N. Winn, *Photonic Crystals*. Princeton, NJ: Princeton Univ. Press, 1995.

[11] P. Villeneuve, S. Fan, and J. D. Joannopoulos, "Microcavities in photonic crystals: Mode symmetry, tunability, and coupling efficiency," *Phys. Rev. B*, vol. 54, pp. 7837–7842, 1996.

[12] S. Lin, V. Hietala, S. Lyo, and A. Zaslavsky, "Photonic band gap quantum well and quantum box structures: A high-$Q$ resonant cavity," *Appl. Phys. Lett.*, vol. 68, pp. 3233–3235, 1996.

[13] D. Labilloy *et al.*, "High-finesse disk microcavity based on a circular Bragg reflector," *Appl. Phys. Lett.*, vol. 73, pp. 1314–1316, 1998.

[14] A. Shaw *et al.*, "Lasing properties of disk microcavity based on a circular Bragg reflector," *Appl. Phys. Lett.*, vol. 75, pp. 3051–3053, 1999.

[15] A. Mekis, M. Meier, A. Dodabalapur, R. E. Slusher, and J. D. Joannopoulos, "Lasing mechanism in two-dimensional photonic crystal lasers," *App. Phys. A*, vol. 69, pp. 111–114, 1999.

[16] M. Imada *et al.*, "Coherent two-dimensional lasing action in surface-emitting laser with triangular-lattice photonic crystal structure," *Appl. Phys. Lett.*, vol. 75, pp. 316–318, 1999.

[17] K. Inoue, M. Sasada, J. Kawamata, K. Sakoda, and J. Haus, "A two-dimensional photonic crystal laser," *Jpn. J. App. Phys.*, vol. 38, pp. L157–L159, 1999.

[18] O. Painter *et al.*, "Two-dimensional photonic band-gap defect mode laser," *Science*, vol. 284, pp. 1819–1821, 1999.

[19] J. Hwang *et al.*, "Room-temperature triangular-lattice two-dimensional photonic bandgap lasers operating at 1.54 $\mu$m," *Appl. Phys. Lett.*, vol. 76, pp. 2982–2984, 2000.

[20] W. D. Zhou, J. Sabarinathan, B. Kochman, E. Berg, O. Qasaimeh, S. Pang, and P. Bhattacharya, "Electrically injected single-defect photonic bandgap surface-emitting laser at room temperature," *Electron. Lett.*, vol. 36, pp. 1541–1542, 2000.

[21] J. L. Jewell, J. P. Harbison, A. Scherer, Y. H. Lee, and L. T. Florez, "Vertical-cavity surface-emitting lasers: Design, growth, fabrication, characterization," *IEEE J. Quantum Electron.*, vol. 27, pp. 1332–1346, 1991.

[22] R. D. Meade, A. M. Rappe, K. D. Brommer, J. D. Joannopoulos, and O. L. Alerhand, "Accurate theoretical analysis of photonic band-gap materials," *Phys. Rev. B*, vol. 48, pp. 8434–8437, 1993.

[23] T. Sondergaard, "Spontaneous emission in two-dimensional photonic crystal microcavities," *IEEE J. Quantum Electron.*, vol. 36, pp. 450–457, 2000.

[24] O. Painter, J. Vuckovic, and A. Scherer, "Defect modes of a two-dimensional photonic crystal in optically thin dielectric slab," *J. Opt. Soc. Amer. B*, vol. 16, pp. 275–285, 1999.

[25] J. M. Dallesasse, N. Holonyak Jr., S. R. Sugg, T. A. Richard, and N. El-Zein, "Hydrolyzation oxidation of $Al_xGa_{1-x}As$-AlAs-GaAs quantum well heterostructures and superlattices," *Appl. Phys. Lett.*, vol. 57, pp. 2844–2846, 1990.

[26] E. Berg and S. W. Pang, "$Cl_2$ plasma passivation of etch induced damage in GaAs and InGaAs with an inductively coupled plasma source," *J. Vac. Sci. Tech. B*, vol. 17, pp. 2745–2749, 1999.

[27] W. D. Zhou, P. Bhattacharya, and O. Qasaimeh, "InP-based cylindrical microcavity light emitting diodes," *IEEE J. Quantum Electron.*, vol. 37, pp. 48–54, Jan. 2001.

[28] A. Chutinan and S. Noda, "Effects of structural fluctuations on the photonic bandgap during fabrication of a photonic crystal: a study of a photonic crystal with a finite number of periods," *J. Opt. Soc. Amer. B*, vol. 16, pp. 1398–1402, 1999.

[29] D. Ochoa *et al.*, "Diffraction of cylindrical Bragg reflectors surrounding an in-plane semiconductor microcavity," *Phys. Rev. B*, vol. 61, pp. 4806–4812, 2000.

[30] R. Coccioli, M. Boroditsky, K. W. Kim, Y. Rahmat-Samii, and E. Yablonovitch, "Smallest possible electromagnetic mode volume in a dielectric cavity," in *IEE Proc. Optoelectron.*, vol. 145, 1998, pp. 391–397.

[31] M. Boroditsky *et al.*, "Spontaneous emission extraction and Purcell enhancement from thin-film 2-D photonic crystals," *J. Lightwave Technol.*, vol. 17, pp. 2096–2112, 1999.

[32] C. H. Henry, R. A. Logan, and F. R. Merritt, "The effect of surface recombination on current in $Al_xGa_{1-x}As$ heterojunctions," *J. Appl. Phys.*, vol. 49, pp. 3530–3542, 1978.

[33] G. Bjork and Y. Yamamoto, "Analysis of semiconductor microcavity lasers using rate equations," *IEEE J. Quantum Electron.*, vol. 27, pp. 2386–2396, 1991.

[34] R. Lee, O. Painter, B. Kitzke, A. Scherer, and A. Yariv, "Emission properties of a defect cavity in a two-dimensional photonic bandgap crystal slab," *J. Opt. Soc. Amer. B*, vol. 17, pp. 629–633, 2000.

[35] O. Painter, A. Husain, A. Scherer, P. T. Lee, I. Kim, J. D. O'Brien, and P. D. Dapkus, "Lithographic tuning of a two-dimensional photonic crystal laser array," *IEEE Photon. Technol. Lett.*, vol. 12, pp. 1126–1128, 2000.


**Wei Dong Zhou** (S'98) received the B.S. and M.E. degrees (Hons.) in electrical engineering from Tsinghua University, Beijing, China, in 1993 and 1996, respectively. He is currently working toward Ph.D. degree in electrical engineering at the University of Michigan at Ann Arbor.

His research work in the area of optoelectronics a includes design, fabrication, and characterization of optical microcavities, photonic bandgap materials, and microcavity surface emitters. He is also interested in the work on high-speed dynamics of semiconductor lasers, low-power phototransceivers, and OEICs.

**Jayshri Sabarinathan** (S'01) received the B.S.E degree in electrical engineering and engineering physics and the M.S.E degree in electrical engineering in 1997 and 1999, respectively, from the University of Michigan at Ann Arbor, where she is currently working toward the Ph.D. degree in optoelectronics.

Her current research interests include the design and fabrication of III-V semiconductor based 3-D photonic crystals, 2-D photonic crystal defect microcavities, and microfluidic sensors.

Ms. Sabarinathan is a member of Eta Kappa Nu (HKN) and Tau Beta Pi engineering honor societies.

**Pallab Bhattacharya** (M'78–SM'83–F'89) received the Ph.D. degree from the University of Sheffield, Sheffield, U.K., in 1978.

He is the James R. Mellor Professor of Engineering and Professor of Electrical Engineering and Computer Science at the University of Michigan at Ann Arbor, which he joined in 1983. His teaching and research interests include molecular beam epitaxy of elemental and III-V compound semiconductors, materials characterization, electronic and optoelectronic devices, and optoelectronic integrated circuits. From 1978 to 1983, he was on the faculty of Oregon State University at Corvallis. He was an Invited Professor at the Ecole Polytechnic Federale, Lausanne, Switzerland, from 1981 to 1982. He has published over 300 technical articles in archival journals, authored the textbook *Semiconductor Optoelectronic Devices* (Englewood Cliffs, HJ: Prentice-Hall, 1994, 1st ed., and 1997, 2nd ed), and edited *Properties of Lattice-Matched and Strained InGaAs* (London, U.K.: INSPEC, 1993) and *Properties of III-V Quantum Wells and Superlattices* (London, U.K.: INSPEC, 1996).

Dr. Bhattacharya is an Editor of the IEEE TRANSACTIONS ON ELECTRON DEVICES. He has served on the Advisory Board of the Electrical and Communications Systems Division of the National Science Foundation and on several other committees and panels in government, industry, and technical conferences. He received the Parker Rhodes Scholarship from the University of Sheffield, the Research Excellence Award from the University of Michigan, the Alexander von Humboldt Award, the John Simon Guggenheim Award, the IEEE (LEOS) Distinguished Lecturer Award, the SPIE Technology Achievement Award, the IEEE (EDS) Paul Rappaport Award, the IEEE (LEOS) Engineering Achievement Award, the University of Michigan Distinguished Faculty Achievement Award, and the S. S. Attwood Award from the University of Michigan. He is a Fellow of the Optical Society of America and a member of the American Physical Society and Sigma Xi.

**Boaz Kochman** received the B.S. degree in engineering physics and computer science from Cornell University, Ithaca, NY, and the M.S. degree in electrical engineering from the University of Michigan at Ann Arbor, where he is currently working toward Ph.D. in electrical engineering.

His research focuses on quantum transport and single-electron phenomena.

**Erik W. Berg**, photograph and biography not available at the time of publication.

**Pei-Chen Yu** received the B.S. degree in electrophysics and M.S. degree in electrooptical engineering from National Chiao-Tung University, Taiwan, in 1996 and 1998, respectively. She is currently working toward the Ph.D. degree in electrical engineering at the University of Michigan at Ann Arbor.

Her research involves optoelectronic device design and modeling of the interaction between atom and field in active structures.

**Stella W. Pang** (S'81–M'82–SM'91–F'99) received the Ph.D. degree in electrical engineering and computer science from Princeton University, Princeton, NJ, in 1981.

She has been a Professor of Electrical Engineering and Computer Science at the University of Michigan at Ann Arbor since 1990. From 1981 to 1989, she was with Lincoln Laboratory, Massachusetts Institute of Technology, Cambridge, MA, working on submicrometer technology for microelectronic applications. Her research interests include nanofabrication technology, dry etching, dry deposition, and surface modifications for microelectromechanical, microelectronic, and optical devices. She has contributed to over over 250 technical papers, book chapters, and presentations.

Dr. Pang has served as conference organizer for the IEEE Electrochemical Society, the Material Research Society, the American Vacuum Society, and SPIE. She is Fellow of ECS and AVS.